






Shock-driven synchrotron radio emission from the 2021 outburst of RS Ophiuchi

Nayana A. J. ^{1,2}★, G. C. Anupama ², Nirupam Roy,³ Dipankar P. K. Banerjee,⁴ Kulinder Pal Singh ⁵,
L. S. Sonith ² and U. S. Kamath ²

¹Department of Astronomy, University of California, Berkeley, CA 94720-3411, USA

²Indian Institute of Astrophysics, II Block, Koramangala, Bangalore 560034, India

³Department of Physics, Indian Institute of Science, Bangalore 560012, India

⁴Astronomy & Astrophysics Division, Physical Research Laboratory, Ahmedabad 380009, India

⁵Department of Physical Sciences, IISER Mohali, Knowledge City, Sector 81, Manauli PO, SAS Nagar, Punjab 140306, India

Accepted 2024 January 8. Received 2023 December 1; in original form 2023 May 22

ABSTRACT

We present low-frequency radio observations of the Galactic symbiotic recurrent nova RS Ophiuchi during its 2021 outburst. The observations were carried out with the upgraded Giant Metrewave Radio Telescope spanning a frequency range of 0.15–1.4 GHz during 23–287 d post the outburst. The average value of the optically thin spectral index is $\alpha \sim -0.4$ ($F_\nu \propto \nu^\alpha$), indicating a non-thermal origin of the radio emission at the observed frequencies. The radio light curves are best represented by shock-driven synchrotron emission, initially absorbed by a clumpy ionized circumbinary medium. We estimate the mass-loss rate of the red giant companion star to be $\dot{M} \sim 7.5 \times 10^{-8} M_\odot \text{ yr}^{-1}$ for an assumed stellar wind velocity of 20 km s^{-1} . The 0.15–1.4 GHz radio light curves of the 2021 outburst are systematically brighter than those of the 2006 outburst. Considering similar shock properties between the two outbursts, this is indicative of a relatively higher particle number density in the synchrotron emitting plasma in the current outburst.

Key words: radiation mechanisms: non-thermal – radio continuum: general – transients: novae.

1 INTRODUCTION

RS Ophiuchi is a Galactic symbiotic recurrent nova system composed of a primary white dwarf that accretes matter from its red giant companion. The nova has undergone seven reported outbursts, at somewhat irregular intervals, in the years 1898, 1933, 1958, 1967, 1985, 2006, and 2021 (Schaefer 2010, and references therein). The 2021 outburst was discovered on 2021 August 08.93 (UT) in the optical bands.¹ The nova brightened to a visual magnitude of 4 mag, which is ~ 1000 times brighter than its quiescent magnitude. Subsequently, the nova showed luminous emission over a wide range of frequencies from radio to the very high energy (VHE) γ -rays.

γ -ray emission was detected with Fermi-LAT (Cheung et al. 2022; Zheng et al. 2022), H.E.S.S. (H. E. S. S. Collaboration 2022), and MAGIC (Acciari et al. 2022) telescopes in the GeV–TeV energy regime, marking the first detection of VHE emission from a nova. The GeV to TeV emission has been interpreted under either a hadronic (Acciari et al. 2022; H. E. S. S. Collaboration 2022; Zheng et al. 2022; Diesing et al. 2023) or a leptohadronic (De Sarkar et al. 2023) particle acceleration scenario. The evolution of the hard X-ray emission, arising from shock interaction between the nova ejecta and the red giant wind, was found to be similar to the 2006 outburst

(Page et al. 2022). On the other hand, the evolution in the soft X-ray, during the super soft state (SSS), was found to be fainter compared to the 2006 outburst (Page et al. 2022). High resolution X-ray spectra observed during $t \sim 18$ –21 d with *Chandra* and *XMM-Newton* (Orion et al. 2022) indicated the presence of multiple thermal components over a range of temperatures $T = 0.07$ –3.4 keV.

Ness et al. (2023) analysed the X-ray grating spectra of both the 2006 and 2021 outbursts and concluded the low SSS emission in 2021 to be due to higher absorption in the line of sight compared to that of 2006. The early optical spectrum of the 2021 outburst showed emission lines of full width at half-maximum $\sim 2900 \text{ km s}^{-1}$ (Munari & Valisa 2021b). The ejecta accelerated to velocities $\sim 4700 \text{ km s}^{-1}$ (Mikolajewska et al. 2021) in the first two days followed by decreasing line velocities indicating deceleration (Pandey et al. 2022). The optical photometric and spectroscopic evolution of the 2021 outburst presented by Munari & Valisa (2021a, 2022) indicate it to be very similar to that of previous outbursts. The morphokinematic modelling of H α emission lines suggested a bipolar ejecta geometry (Pandey et al. 2022) similar to that seen during the 2006 outburst (Rupen, Mioduszewski & Sokolowski 2008).

Radio emission was detected from RS Ophiuchi from ~ 1 d post-outburst at multiple frequencies (0.15–35 GHz; Nayana et al. 2021; Sokolovsky et al. 2021; Williams et al. 2021; de Ruiter et al. 2023). Munari et al. (2022) presented the European Very Large Baseline Interferometry Network (EVN) observations of RS Oph at 5 GHz and reported the total extension of the radio-emitting region to

* E-mail: nayana.aj@iiaap.res.in, nayana@berkeley.edu

¹<http://ooruri.kusastro.kyoto-u.ac.jp/mailarchive/vsnet-alert/26131>

be ~ 90 mas at $t \sim 34$ d. Radio emission from novae could be thermal free-free emission from hot ionized ejecta and/or non-thermal synchrotron emission from shocks. Low-frequency radio emission are synchrotron-dominated and are critical in understanding the properties of circumbinary medium (CBM) and shocks.

In this paper, we present extensive low-frequency (0.15–1.4 GHz) radio observations and modelling of RS Ophiuchi during its 2021 outburst. The paper is organized as follows: We present the radio observations and data reduction in Section 2. Radio light curves and spectra are presented in Section 3 and the radio emission model is explained in Section 5. We discuss our results in Sections 6 and 7. We summarize our findings in Section 8.

Throughout this paper, we use the time of nova outburst, 2021 August 08.5 UT (Munari & Valisa 2021a) as the reference time. All times t mentioned are with respect to this reference epoch.

2 UGMRT OBSERVATIONS AND DATA REDUCTION

Upgraded Giant Metrewave Radio Telescope (uGMRT) observations of RS Ophiuchi were carried out from 2021 August 31 ($t \sim 23$ d) to 2022 May 23 ($t \sim 287$ d) under Director’s Discretionary Time (DDTC204, DDTC205, DDTC207, DDTC211, and DDTC222) and regular GTAC proposals (42_083). The observations were done in band-2 (125–250 MHz), band-3 (250–500 MHz), band-4 (550–850 MHz), and band-5 (1000–1460 MHz). The data were recorded with an integration time of 10 s in the standard continuum mode. We used a processing bandwidth of 400 MHz in bands 4 and 5, 200 MHz in band 3, and 100 MHz in band 2, split into 2048 channels. 3C286, 3C48, and 3C147 were used as flux density calibrators. J1822–096 and J1743–038 were used as the phase calibrators.

The Astronomical Image Processing Software (AIPS; Greisen 2003) was used for data reduction, following standard radio continuum imaging analysis procedures (Nayana et al. 2017). The data were initially inspected for non-working antennae and radio frequency interference (RFI) affected channels and corrupted data were flagged. The calibration was done using a central channel and the solutions were applied to the entire band. The fully calibrated source data were imaged using AIPS task IMAGR. We performed a few rounds of phase-only self-calibration to improve the image quality.

We detected radio emission from RS Ophiuchi at all frequencies and the emission was unresolved in all the maps. We estimated the flux density and error of the target source by fitting a Gaussian at the source position using AIPS task JMFIT. The size of the fitted Gaussian is consistent with that of a point source in all the maps. Resolutions of the radio maps are typically 5×2 , 7×5 , 13×7 , and 25×17 arcsec² in bands-5, 4, 3, and 2, respectively. In addition to the errors on flux densities from task JMFIT, we add (in quadrature) a 10 per cent error in bands-3, 4, and 5 and a 15 per cent error in band-2 to account for the calibration uncertainties. The flux densities at multiple epochs are listed in Table 1.

3 RADIO LIGHT CURVES AND SPECTRA

The uGMRT light curves at 1.36, 0.69, 0.44, and 0.15 GHz are presented in Fig. 1 (left panel). The 1.36 and 0.69 GHz light curves show a steady decline from a possible maximum at $t \lesssim 20$ d. The 0.44 GHz light curve peaks slightly later (at $t \sim 35$ d) than that of the 1.36 and 0.69 GHz light curves. The first three epochs of 0.15 GHz flux measurements are possibly indicating a rising phase, whereas the light curve is in the declining phase at $t \sim 287$ d. However, we note that the error bars on these flux measurements are

Table 1. Details of the uGMRT observations of RS Ophiuchi in its 2021 outburst.

Date of observation (UT)	Time ^a (d)	Frequency (GHz)	Flux density (mJy)
2021 Sep 02.53	25.03	1.36	85.10 ± 8.60
2021 Sep 14.73	37.23	1.37	61.00 ± 6.30
2021 Sep 26.69	49.19	1.36	43.10 ± 4.70
2021 Sep 31.67	54.17	1.36	45.90 ± 4.60
2021 Oct 05.34	57.84	1.36	60.40 ± 6.00
2022 Feb 05.26	180.76	1.36	13.10 ± 1.31
2022 Apr 25.03	259.53	1.36	09.90 ± 0.99
2021 Aug 31.67	23.17	0.69	77.50 ± 8.00
2021 Sep 17.67	40.17	0.69	78.00 ± 7.90
2021 Sep 21.72	44.22	0.69	63.00 ± 6.40
2021 Oct 01.58	54.08	0.69	72.10 ± 7.70
2021 Oct 08.41	60.91	0.66	58.90 ± 6.10
2021 Nov 15.42	98.92	0.64	43.30 ± 4.40
2021 Nov 26.25	109.75	0.69	23.90 ± 2.60
2021 Dec 06.15	119.65	0.69	26.90 ± 3.00
2021 Dec 18.21	131.71	0.69	25.00 ± 2.50
2021 Dec 31.26	144.76	0.69	21.30 ± 2.30
2022 Jan 10.08	154.58	0.69	16.50 ± 1.80
2022 Feb 08.19	183.69	0.69	16.49 ± 1.71
2022 Mar 01.04	204.54	0.69	13.36 ± 1.37
2022 Mar 28.95	232.45	0.69	11.55 ± 1.17
2022 Apr 24.98	259.48	0.62	10.14 ± 1.02
2021 Sep 05.51	28.01	0.40	73.10 ± 11.20
2021 Sep 16.70	39.20	0.46	71.70 ± 7.80
2021 Sep 21.38	43.88	0.46	85.10 ± 12.80
2021 Sep 30.62	53.12	0.45	80.00 ± 8.10
2021 Oct 03.42	55.92	0.46	75.80 ± 11.50
2021 Nov 15.49	98.99	0.40	48.30 ± 05.60
2021 Nov 26.33	109.83	0.44	38.43 ± 3.85
2021 Dec 07.46	120.96	0.45	37.15 ± 3.74
2021 Dec 18.46	131.96	0.43	29.68 ± 3.07
2021 Dec 31.34	144.84	0.44	28.06 ± 2.86
2022 Jan 10.32	154.82	0.44	23.91 ± 2.41
2022 Feb 08.00	183.81	0.46	18.40 ± 1.93
2022 Mar 01.12	204.62	0.44	14.46 ± 1.48
2022 Mar 29.04	232.54	0.44	13.12 ± 1.34
2022 May 22.85	287.35	0.44	08.93 ± 1.22
2021 Sep 30.53	53.03	0.147	33.20 ± 8.20
2021 Oct 03.34	55.84	0.147	31.40 ± 6.60
2021 Oct 08.38	60.88	0.146	48.90 ± 10.80
2022 May 22.91	287.41	0.147	26.80 ± 5.10

Note. ^aThis column indicates the time from the nova outburst, i.e. 2021 Aug 08.5 UT (Munari & Valisa 2021a).

large. de Ruiter et al. (2023) presented LOFAR (54 and 154 MHz) and MeerKAT (0.82 and 1.28 GHz) observations of RS Ophiuchi during $t \sim 2$ –223 d post the outburst. The combined GMRT + LOFAR + MeerKAT observations suggest the radio light-curve evolution to be an initial steep rise to peak followed by a steady decline where higher frequencies trace the peak first (see Fig. 2). This kind of light-curve evolution is similar to that seen in radio supernovae (Weiler et al. 2002).

The 1.28 GHz light curve presented in de Ruiter et al. (2023) shows a plateau between $t \sim 10$ and 40 d. Our band-5 light curve does not show such a flattening towards the peak due to sparse temporal sampling, covering only two measurements between 10 and 40 d.

The near-simultaneous spectral indices, α ($F \propto \nu^\alpha$), are estimated at multiple epochs (see Fig. 1 and Table 2). The spectral index between 1.36/0.69 GHz is -0.67 ± 0.22 at $t \sim 54$ d and gradually

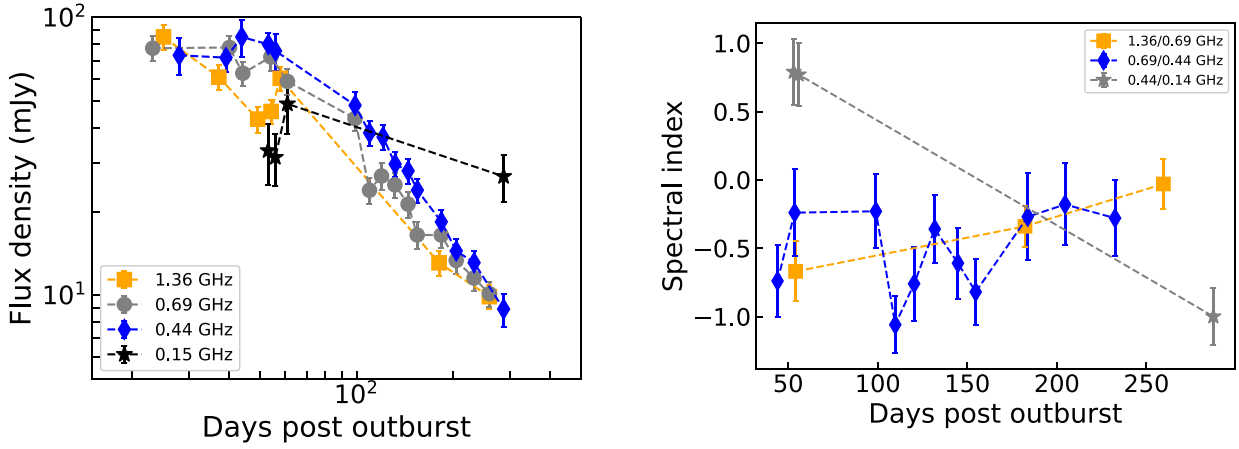


Figure 1. Left panel: The uGMRT light curves of RS Ophiuchi in its 2021 outburst at 1.36, 0.69, 0.44, and 0.15 GHz. Right panel: The near simultaneous spectral indices between 1.36/0.69, 0.69/0.44, and 0.44/0.15 GHz.

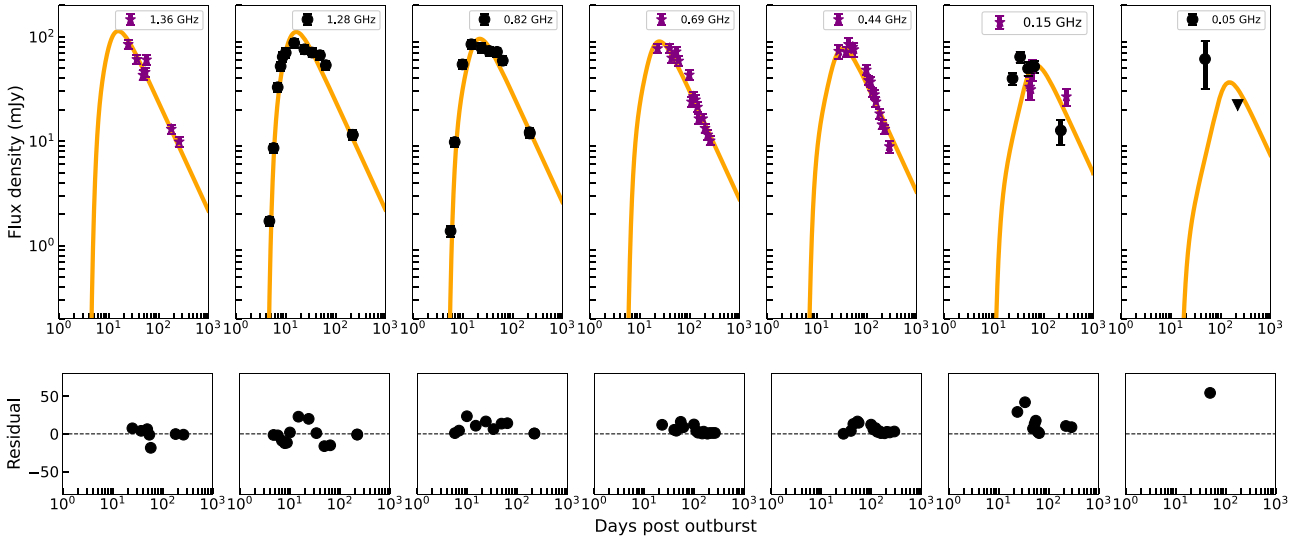


Figure 2. Low-frequency radio light curves of RS Ophiuchi in its 2021 outburst. The data points include flux density measurements from our uGMRT observations and the measurements reported by de Ruiter et al. (2023) at $t > 5$ d. The star symbols denote the uGMRT flux density measurements and the circles denote the flux measurements reported by de Ruiter et al. (2023). The solid curves represent the best-fitting single-component synchrotron emission model (Weiler et al. 2002) as described by equations (2), (3), and (4) (see Section 5). The bottom panels show the residuals defined as $F_o - F_{\text{mod}}$, where F_o is the observed flux density and F_{mod} is the modeled flux value.

approaches a value $\alpha \sim -0.03$ by $t \sim 259$ d. The average value of spectral index between 0.69 and 0.44 GHz is ~ -0.6 during $t \sim 44$ –183 d, and flattens to $\alpha \sim -0.2$ to -0.3 during $t \sim 204$ –232 d. The 0.44/0.15 GHz spectral indices are ~ 0.8 in the rising phase of the light curve and then become $\alpha \sim -1$ at $t \sim 287$ d. The negative spectral indices suggest that the radio emission is predominantly non-thermal (synchrotron) at the observed frequencies. However, the contribution from non-thermal processes seems to decrease at epochs $t \gtrsim 204$ d. This could possibly be due to the shock deceleration and the shock expanding to a rarified CBM further away from the binary system.

4 BRIGHTNESS TEMPERATURE

Synchrotron radio emission is characterized by high brightness temperature ($T_B \gtrsim 10^5$ – 10^6 K), significantly above the maximum brightness temperature of a photoionized thermal gas (10^4 K). We

calculate the brightness temperature of the observed radio flux densities using the following equation (Chomiuk et al. 2021):

$$\frac{T_B}{(K)} = 1200 \left(\frac{F_\nu}{(\text{mJy})} \right) \left(\frac{\nu}{(\text{GHz})} \right)^{-2} \left(\frac{\theta}{(\text{arcsec})} \right)^{-2}. \quad (1)$$

Here, F_ν is the radio flux density at frequency ν , and θ is the angular size of the radio-emitting region. Estimation of the brightness temperature requires knowing the velocity of the ejected material and hence the geometry and kinematics of the ejecta. High-resolution *HST* and radio imaging of both the 2006 and 2021 outbursts show that the nova ejecta is bipolar (or equivalently hourglass) in shape (O’Brien et al. 2006; Bode et al. 2007; Munari et al. 2022). Specifically, radio imaging of the 2021 eruption (Munari et al. 2022) supports a geometric model wherein the leading edges of the bipolar lobes have a space velocity of 7550 km s^{-1} at $t \sim 34$ d. In a bipolar morphology, since the velocity flow is expected to be homologous

Table 2. Near simultaneous radio spectral indices of RS Ophiuchi in its 2021 outburst.

Time ^a (d)	Spectral indices		
	(1.4 and 0.69 GHz)	(0.69 and 0.44 GHz)	(0.44 and 0.15 GHz)
54.13	-0.67 ± 0.22	-	-
182.22	-0.34 ± 0.15	-	-
259.51	-0.03 ± 0.18	-	-
44.05	-	-0.74 ± 0.26	-
53.60	-	-0.24 ± 0.32	-
98.96	-	-0.23 ± 0.27	-
109.79	-	-1.06 ± 0.21	-
120.31	-	-0.76 ± 0.27	-
131.84	-	-0.36 ± 0.25	-
144.80	-	-0.61 ± 0.26	-
154.70	-	-0.82 ± 0.24	-
183.75	-	-0.27 ± 0.32	-
204.58	-	-0.18 ± 0.30	-
232.49	-	-0.28 ± 0.28	-
53.07	-	-	0.79 ± 0.31
55.88	-	-	0.77 ± 0.45
287.38	-	-	-1.00 ± 0.26

Note. ^aThis column indicates the time from the nova outburst, i.e. 2021 Aug 08.5 UT (Munari & Valisa 2021a).

(i.e. $v \propto r$), the leading edge of the bipolar lobes (having the largest r) has the highest velocity, while the other material, especially the constricted material at the waist, has lower velocities. As a rough approximation, we assume the waist is constricted to the extent that the material there has a space velocity of $\sim 3780 \text{ km s}^{-1}$, i.e. half of that of the leading edge that has a velocity of 7550 km s^{-1} . We thus adopt a simplified, mean space velocity of 5660 km s^{-1} for the entire ejecta at $t \sim 34 \text{ d}$. Mondal et al. (2018) reported a velocity deceleration index of the nova ejecta $v \propto t^{-0.66}$ at $t \sim 5\text{--}70 \text{ d}$ during the 2006 outburst of RS Ophiuchi. The velocity remains roughly constant up to $t \sim 247 \text{ d}$ after a slight increase around $t \sim 80 \text{ d}$. We use θ from VLBI observations (Munari et al. 2022) at $t \sim 34 \text{ d}$ and use the velocity deceleration indices from Mondal et al. (2018) to calculate the angular size at later epochs. The brightness temperatures corresponding to our flux density measurements are $\sim 10^5\text{--}10^8 \text{ K}$ for an adopted distance of $2.68_{-0.15}^{+0.17} \text{ Kpc}$ (Gaia DR3; Bailer-Jones et al. 2021). Based on the estimated spectral indices and high brightness temperatures, we conclude that the radio emission is predominantly non-thermal at the observed frequencies.

5 RADIO EMISSION MODEL

Low-frequency radio light curves of RS Ophiuchi can be represented by adopting the synchrotron emission model from Weiler et al. (2002). According to this model, the outburst ejecta plows into the dense red giant wind driving a forward shock. Particles are accelerated at the shock via diffusive shock acceleration and emit synchrotron radiation. Initially, the emission is suppressed via free-free absorption by a homogeneous and clumpy CBM in the line of sight. The spectral and temporal evolution of radio flux densities can be represented as

$$F(\nu, t) = K_1 \left(\frac{\nu}{1 \text{ GHz}} \right)^\alpha \left(\frac{t}{20 \text{ d}} \right)^\beta \times \exp(-\tau_{\text{homog}}) \left[\frac{1 - \exp(-\tau_{\text{clumps}})}{\tau_{\text{clumps}}} \right]. \quad (2)$$

Here, K_1 denotes the flux density normalization constant and t denotes the time since the outburst in days. β is the temporal decay

index of flux densities in the optically thin regime. τ_{homog} and τ_{clumps} represent the optical depths due to homogeneous and clumpy CBM, respectively.

$$\tau_{\text{homog}} = K_2 \left(\frac{\nu}{1 \text{ GHz}} \right)^{-2.1} \left(\frac{t}{20 \text{ d}} \right)^\delta, \quad (3)$$

$$\tau_{\text{clumps}} = K_3 \left(\frac{\nu}{1 \text{ GHz}} \right)^{-2.1} \left(\frac{t}{20 \text{ d}} \right)^{\delta'}. \quad (4)$$

In the above equations, K_2 and K_3 are the optical depths due to homogeneous and clumpy CBM, respectively, at 1 GHz on $t = 20 \text{ d}$. δ and δ' denote the temporal indices of optical depths due to homogeneous and clumpy absorbing medium, respectively.

We model the radio flux density measurements using equations (2), (3), and (4) keeping K_1 , K_2 , K_3 , α , β , δ , and δ' as free parameters. In addition to the uGMRT flux measurements, data from de Ruiter et al. (2023) are also used. Since it is likely that data at $t < 5 \text{ d}$ are due to a residual synchrotron component from previous outbursts (de Ruiter et al. 2023), only the data from $t > 5 \text{ d}$ are included for modelling. The PYTHON EMCEE package (Foreman-Mackey et al. 2013) that adopts Markov chain Monte Carlo (MCMC) method is used to execute the fit. We chose 5000 steps and 32 walkers to explore the parameter space to get the best-fitting parameters (68 per cent confidence interval). The best-fitting model along with the observed flux values are plotted in Fig. 2 and the best-fitting parameters are listed in Table 3. The reduced chi-square value for the best-fitting model is $\chi_\mu^2 = 3.7$. We also modelled the data including the flux measurements at $t < 5 \text{ d}$ and the fit resulted in a much higher reduced $\chi_\mu^2 = 6.4$.

The best-fitting optically thin spectral and temporal indices are $\alpha = -0.37_{-0.04}^{+0.05}$ and $\beta = -1.04_{-0.03}^{+0.03}$, respectively, roughly similar to the values seen in radio supernovae (Weiler et al. 2002). The best-fitting optical depth normalization parameters due to uniform and clumpy medium are $K_2 = 1.68 \times 10^{-3}$ and $K_3 = 0.68$, respectively. These values suggest that a clumpy medium in the line of sight is dominating the absorption processes. We repeated the modelling using only GMRT flux measurements and the best-fitting parameters are $K_1 = 171_{-9}^{+11}$, $K_2 = 0.04_{-0.02}^{+0.02}$, $K_3 = 1.33_{-0.25}^{+0.35}$, $\alpha = -0.50_{-0.06}^{+0.06}$,

Table 3. Best-fitting parameters of the synchrotron emission model.

2021 outburst	2006 outburst
$K_1 = 141.25^{+6.97}_{-7.17}$	$K_1 = 79.77^{+14.27}_{-18.55}$
$K_2 = 1.68^{+0.78}_{-0.55} \times 10^{-3}$	$K_2 = 0.07^{+0.07}_{-0.06}$
$K_3 = 0.68^{+0.10}_{-0.10}$	$K_3 = 0.53^{+0.37}_{-0.29}$
$\alpha = -0.37^{+0.05}_{-0.04}$	$\alpha = -0.73^{+0.14}_{-0.13}$
$\beta = -1.04^{+0.03}_{-0.03}$	$\beta = -1.19^{+0.14}_{-0.09}$
$\delta = -5.74^{+0.28}_{-0.30}$	$\delta = -2.32^{+0.66}_{-0.61}$
$\delta' = -3.05^{+0.10}_{-0.12}$	$\delta' = -3.51^{+0.58}_{-0.65}$
$\chi^2 = 3.70$	$\chi^2 = 2.72$

Note. K_1 , K_2 , α , β , δ , and δ' are best-fitting parameters of radio emission model defined by equations (2), (3), and (4) (see Section 5). The modelling (of 2021 outburst) was done including flux density measurements from our uGMRT observations and the ones reported by de Ruiter et al. (2023) at $t > 5$ d.

$\beta = -1.16^{+0.04}_{-0.04}$, $\delta = -1.74^{+0.52}_{-0.53}$, and $\delta' = -3.48^{+0.43}_{-0.38}$. The values of K_1 , α , β , and δ' are roughly similar if we use either GMRT or GMRT + LOFAR + MeerKAT data. However, the value of optical depth normalization parameters (K_2 , K_3) and δ are significantly different. This indicates that including early time data is critically important to pin down the dominant absorption processes.

While the synchrotron model broadly represents the spectral and temporal behaviour of radio light curves, the plateauing towards the peak is not well fitted in the model.

We thus modelled the data in a two-component scenario and found that the fit improved with a reduced chi-square $\chi^2_\mu = 1.5$. The best-fitting model along with the observed flux density measurements are shown in Fig. 3. The best-fitting parameters that represent each of the synchrotron components are: $K_1 \sim 60.3$, $K_2 \sim 1.2 \times 10^{-4}$, $K_3 \sim 2.0 \times 10^{-3}$, $\alpha \sim -0.12$, $\beta \sim -0.8$, $\delta \sim -4.8$, and $\delta' \sim -4.4$ for the first component, and $K_1 \sim 18.4$, $K_2 \sim 4.6 \times 10^{-4}$, $K_3 \sim 1.8$, $\alpha \sim -1.9$, $\beta \sim -2.5$, $\delta \sim -1.1$, and $\delta' \sim -4.5$ for the second component. The flattening or marginal flux density enhancement close to the peak of the light curves is well represented in the two-component model. The first synchrotron component peaks at $t \sim 12$ –20 d, whereas the

contribution from the second component is maximum at $t \sim 24$ –45 d. The flux density enhancement in the light curves above the prediction of a single (first component) synchrotron model during $t \sim 24$ –45 d could be due to a density enhancement in the CBM, as also seen in the 2006 outburst (Kantharia et al. 2007). Alternatively, it could also be a consequence of the complex velocity changes of the ejecta as the shock decelerates, as seen for example during the first 50 d of the 2006 eruption (Fig. 2; Das, Banerjee & Ashok 2006). Velocity changes would result in fluctuations in the kinetic temperature of the shocked gas which would, in turn, affect the non-thermal emission.

An alternative scenario could involve the emergence of additional radio outflow components to the visibility during $t \sim 24$ –45 d. The EVN observations of RS Oph at $t \sim 34.3$ d (Munari et al. 2022) showed three components: one compact central component (CC) and two lobes towards the east and west of the CC (see fig. 2 of Munari et al. 2022). According to the model proposed by Munari et al. (2022), the eastern arc (EA) remains hidden from the observer at early times due to the high free-free opacity caused by the density enhancement in the orbital plane (DEOP). At times $t > t_\tau$ (where t_τ is the time required for EA to expand from the central binary such that the optical depth due to DEOP is ~ 1), the radio emission from EA becomes detectable. As more and more of EA component becomes visible to the observer, the detected flux density will increase. In the 2006 outburst, it was believed that EA became visible during $t \sim 21$ –51 d (O’Brien et al. 2006, 2008; Rupen, Mioduszewski & Sokolowski 2008; Sokolowski, Rupen & Mioduszewski 2008). In the 2021 outburst, the EA is in the emerging phase (outer arc is visible) at $t \sim 34.3$ d (Munari et al. 2022). Considering the similarities between the 2006 and 2021 outbursts in terms of shell velocity and radio morphology, it is very likely that the enhanced flux densities during $t \sim 24$ –45 d are due to the eastern lobe becoming visible to the observer.

Kantharia et al. (2007) presented low-frequency radio light curves of the 2006 outburst of RS Ophiuchi. We use these flux density measurements and model them (in a single component) following the same method as discussed here. The best-fitting values are given in Table 3. We use the results from the single-component modelling and attempt a detailed comparison of the best-fitting parameters with those of the 2006 outburst in Section 6.

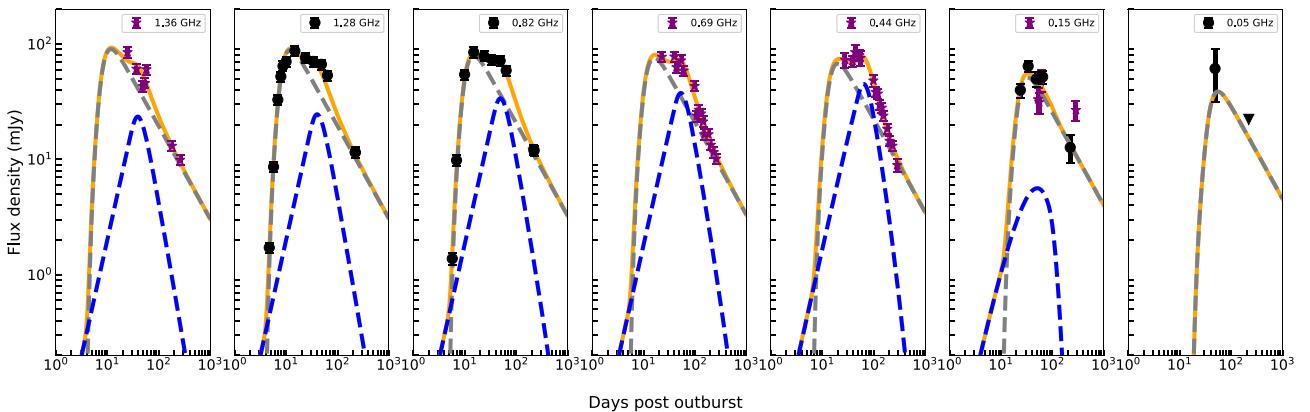


Figure 3. Low-frequency radio light curves of RS Ophiuchi in its 2021 outburst. The data points include flux density measurements from our uGMRT observations and the measurements reported by de Ruiter et al. (2023) at $t > 5$ d. The star symbols denote the uGMRT flux density measurements and the circles denote the flux measurements reported by de Ruiter et al. (2023). The grey and blue dashed curves represent the first and second components of the synchrotron emission model (Weiler et al. 2002), respectively. The solid curves represent the total fit which is the sum of two components. The second component of the 0.05 GHz light curve is out of the plot range (the modeled flux values are too low; $F \ll 1$ mJy).

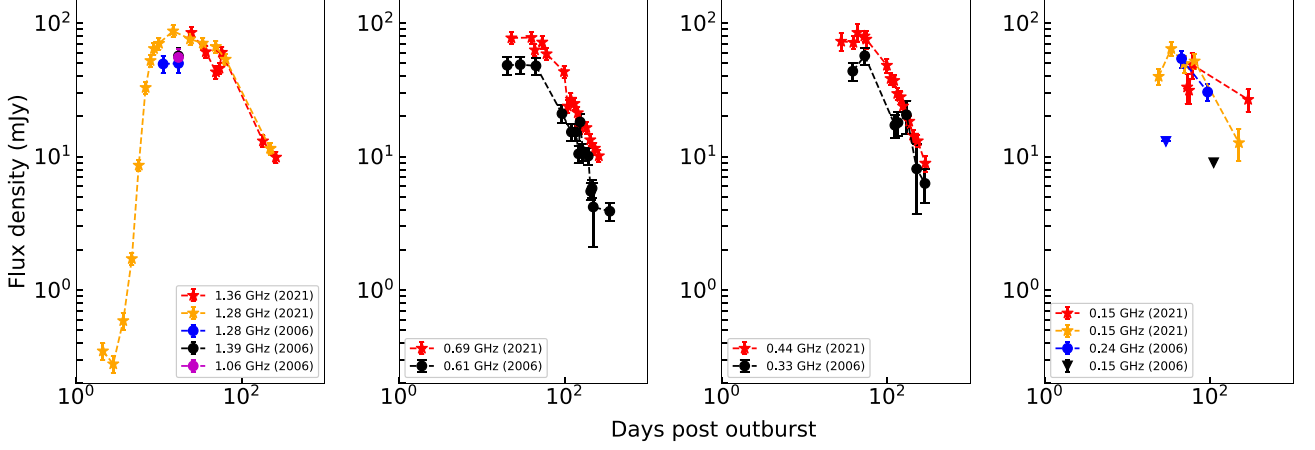


Figure 4. Radio light curves of RS Ophiuchi in its 2006 and 2021 outburst. The uGMRT radio flux density measurements of the 2021 outburst are marked as red star symbols. The flux densities of the 2021 outburst reported in de Ruiter et al. (2023) are marked as orange star symbols. The blue and black filled circles and downward triangles represent the flux densities and limits, respectively, during the 2006 outburst (Kantharia et al. 2007).

5.1 Mass-loss rate

Mass-loss rate (\dot{M}) of the red giant companion can be estimated from the modelled radio light curves (Weiler et al. 1986, 2002).

$$\frac{\dot{M}}{v_{w1}} = 3.0 \times 10^{-6} \langle \tau_{\text{eff}}^{0.5} \rangle m^{-1.5} \left(\frac{v_i}{10^4 \text{ km s}^{-1}} \right)^{1.5} \times \left(\frac{t_i}{45 \text{ d}} \right)^{1.5} \left(\frac{t}{t_i} \right)^{1.5m} \left(\frac{T}{10^4 \text{ K}} \right)^{0.68}. \quad (5)$$

Here, v_{w1} is the stellar wind velocity of the red giant companion in units of 10 km s^{-1} . v_i is the ejecta velocity at t_i days post-outburst. m and T represent the shock deceleration parameter ($m = \delta/3$) and wind electron temperature, respectively. τ_{eff} is the effective optical depth due to a uniform and clumpy absorbing medium (Weiler et al. 2002).

$$\langle \tau_{\text{eff}}^{0.5} \rangle = 0.67 \left[(\tau_{\text{homog}} + \tau_{\text{clumps}})^{1.5} - \tau_{\text{homog}}^{1.5} \right] \tau_{\text{clumps}}^{-1} \quad (6)$$

We estimate the mass-loss rate to be $\dot{M} = 7.5_{-1.6}^{+1.5} \times 10^{-8} M_{\odot} \text{ yr}^{-1}$ for a wind velocity of 20 km s^{-1} and $T = 20000 \text{ K}$ (Weiler et al. 2002). We use $v_i \sim 5660 \text{ km s}^{-1}$ at $t_i = 34 \text{ d}$ (see Section 4). The derived mass-loss rate is in agreement with the typical mass-loss rates (10^{-9} to $10^{-6} M_{\odot} \text{ yr}^{-1}$) of red giant branch (RGB) stars (van Loon et al. 2006; McDonald & van Loon 2007; Origlia et al. 2007) and with that presented in de Ruiter et al. (2023). The above-mentioned formulation of mass-loss rate is originally developed for supernovae (Weiler et al. 2002) assuming a spherical geometry. In the case of RS Oph, the ejecta is bipolar and the estimated \dot{M} value could be a rough approximation.

6 COMPARISON BETWEEN THE RADIO EVOLUTION OF 1985, 2006, AND 2021 OUTBURSTS OF RS OPHIUCHI

Radio emission was detected and monitored from the 1985 (Hjellming et al. 1986) and 2006 (Kantharia et al. 2007; Eyres et al. 2009) outbursts of RS Ophiuchi. In this section, we compare the properties of radio emission from previous outbursts with that of 2021 to understand the evolution of the system in terms of shock energetics and the CBM.

Hjellming et al. (1986) presented radio observations spanning $t \sim 29\text{--}370 \text{ d}$ post the 1985 outburst at frequencies 1.49, 4.85, 14.94, and 22.46 GHz with the Very Large Array (VLA). Radio emission from the 2006 outburst of RS Ophiuchi was detected at frequencies 0.24, 0.33, 0.61, 1.49, 4.89, 6.0, 14.96, and 22.48 GHz (Narumi et al. 2006; Kantharia et al. 2007; Eyres et al. 2009). In both outbursts, two spectral components were identified, one with a negative spectral index between 1.4/5 GHz and below, and the other with a positive spectral index above 5 GHz. The GMRT observations of the 2006 outburst were carried out by Kantharia et al. (2007) during $t \sim 13\text{--}110 \text{ d}$ post-discovery at frequencies 1.39, 1.28, 1.06, 0.61, 0.33, 0.24, and 0.15 GHz. Radio emission was detected at all frequencies except at $\nu = 0.15 \text{ GHz}$ at $t \sim 110 \text{ d}$ with a 3σ flux density limit of 27 mJy.

We compile all published low-frequency ($\nu \leq 1.4 \text{ GHz}$) radio observations of 1985 and 2006 outbursts to investigate the evolution of shock-driven synchrotron emission over successive outbursts. Fig. 4 shows the radio light curves at $\nu \sim 0.15\text{--}1.4 \text{ GHz}$ of RS Ophiuchi in its 2006 and 2021 outbursts and Fig. 5 shows the 1.4 GHz light curves of 1985, 2006, and 2021 outbursts.

When we compare the low-frequency radio light curves of the 2006 and 2021 outbursts, two characteristics are particularly striking.

- (i) The radio flux densities during the 2021 outburst are systematically higher than those of the 2006 outburst.
- (ii) Radio emission at 0.15 GHz is detected from $t \sim 24$ to 287 d at nine epochs during the 2021 outburst. Radio observations at 0.15 GHz were carried out only at a single epoch ($t \sim 110 \text{ d}$) in the 2006 outburst that resulted in non-detection with a 3σ flux density limit of $F < 27 \text{ mJy}$.

6.1 Brighter synchrotron emission during the 2021 outburst

The observed peak flux densities of the bands 5, 4, and 3 light curves in the 2021 outburst are $\sim 85, 78,$ and 85 mJy , respectively. The corresponding values in the 2006 outburst are $\sim 57, 49,$ and 57 mJy , respectively (Kantharia et al. 2007), about 1.5–1.6 times lower. If we compare the flux densities at higher frequencies between 2021 (Sokolovsky et al. 2021) and 2006 outbursts (Eyres et al. 2009), this trend seems to be broad-band.

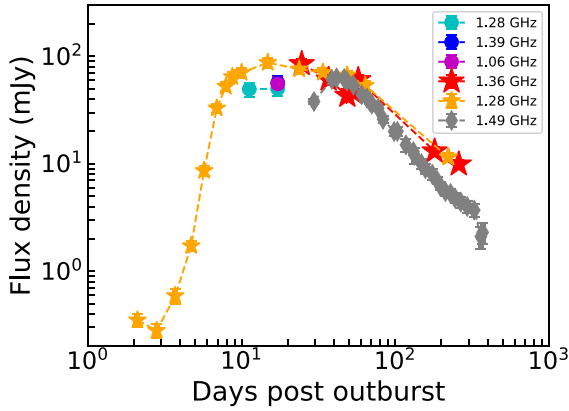


Figure 5. Radio light curves of RS Ophiuchi in its 1985, 2006, and 2021 outburst. The uGMRT radio flux density measurements of the 2021 outburst are marked as red star symbols. The flux densities of the 2021 outburst reported by de Ruiter et al. (2023) are marked as orange star symbols. The blue, cyan, and magenta filled circles represent the flux densities during the 2006 outburst (Kantharia et al. 2007). The diamonds denote the flux density measurements from the 1985 outburst (Hjellming et al. 1986).

The key dependences on the synchrotron emissivity [$J(\nu)$] are (equation 8.89; Longair 2011)

$$J(\nu) \propto N_0 B^{(p+1)/2} \nu^{-(p-1)/2}, \quad (7)$$

where the power-law distribution of electron energies is represented as $N(E)dE = N_0 E^{-p} dE$. Here, $N(E)dE$ is the number density of electrons of energies between E and $E + dE$. Thus a higher synchrotron radio flux density could be due to more synchrotron emitting electrons in the emitting region and/or due to a higher magnetic field.

Assuming the amplified post-shock magnetic field is in equipartition with the relativistic electrons in the radio-emitting region (Chevalier & Fransson 2006; Chugai 2010), the magnetic field can be written as (Chomiuk et al. 2012)

$$B = \sqrt{8\pi \epsilon_B \mu m_H n_{\text{CBM}} v^2}. \quad (8)$$

Here, n_{CBM} is the particle number density in the CBM and v is the shock velocity. Munari et al. (2022) reported the size and expansion velocity of the radio-emitting region at $t \sim 34$ d in the 2021 outburst and mentioned that the size is remarkably similar in the case of 2006 outburst at similar epochs. The hard X-ray emission and its temporal evolution are also reported to be broadly similar between the two outbursts (Page et al. 2022). Both these observations are indicative of similar shock velocities during the 2006 and 2021 outbursts. Thus the higher synchrotron brightness in the 2021 outburst could be due to a higher density of the CBM. The synchrotron radio flux density can be represented in terms of electron number density in the synchrotron plasma as $F \propto n_e^{(p+5)/4}$, where p is related to the optically thin spectral index as $\alpha = (p-1)/2$. Thus a 1.5–1.6 times increase in synchrotron flux densities during the 2021 outburst compared to that of 2006 could indicate a ~ 30 per cent increase in n_e considering the shock velocity and magnetic field are the same during both outbursts.

We detect 0.15 GHz radio emission at $t \sim 52, 55, 60,$ and 287 d post the 2021 outburst of RS Ophiuchi. de Ruiter et al. (2023) reported radio emission at 0.15 GHz at $t \sim 24, 34, 49, 65,$ and 223 d post-outburst. Observations at this frequency at a single epoch ($t \sim 110$ d) during the 2006 outburst resulted in non-detection with a 3σ flux density limit of 27 mJy. However, during the 2021 outburst, the best-fitting model predicts a flux density of ~ 44 mJy at 110 d, which

is significantly higher than the flux density limit during the 2006 outburst. This could either be indicative of an early turn-on of the 0.15 GHz radio emission in the 2021 outburst or be due to the intrinsically brighter synchrotron emission in 2021 compared to that of 2006.

We now look at the published 1.4 GHz radio observations during the 1985 outburst along with those of 2006 and 2021 in Fig. 5. The radio emission is brightest in the 2021 outburst whereas the 2006 and 1985 outbursts show roughly similar flux values. The time of peak of the 1.4 GHz light curve (t_p) is not well constrained in the 1985 outburst due to sparse sampling of the light curve at $t < 20$ d (see fig. 1 of Hjellming et al. 1986). We assume the peak of the 1.4 GHz light curve in the 1985 outburst to be $t_p \lesssim 20$ d, similar to that of the 2006 ($t_p \sim 15$ d) and 2021 ($t_p \sim 15$ d) outbursts. The 0.325 GHz emission was not detected from the 1985 outburst at $t \sim 48$ d down to a flux density limit of 5 mJy whereas 0.325 GHz emission was detected at $t \sim 38$ d in the 2006 outburst with a flux density of 43.7 mJy. The non-detection of 0.325 GHz emission are indications of higher foreground absorption in 1985 than in 2006 (Kantharia et al. 2007).

6.2 Evolution of optical depths due to uniform and clumpy absorbing medium

We investigate the evolution of optical depth due to uniform and clumpy components of the absorbing medium during the 2006 and 2021 outbursts from the best-fitting modelled parameters. Table 4 shows the values of τ_{homo} , τ_{clumps} , and τ_{eff} in the 2006 and 2021 outbursts at the time of the peak of the 1.36, 0.69, 0.44, and 0.15 GHz light curves in 2021 outburst. The optical depth due to the inhomogeneous component of the absorbing medium is systematically higher in 2021 than in 2006 suggesting that the clumpiness in the CBM has increased from 2006 to 2021.

7 A COMPREHENSIVE PICTURE

Shock-driven synchrotron radio emission from multiple outbursts of RS Ophiuchi shows differences in radio brightness. It is important to tie down these differences with observational characteristics at other frequencies (optical, X-ray, γ -rays) and theoretical models to build a comprehensive picture.

The optical light curves and evolution between 2006 and 2021 outbursts are almost identical, indicating that the ejecta mass, the mass of the white dwarf, and ejecta velocities are broadly the same (Page et al. 2022). The hard X-ray emission (> 1 keV) during the 2021 and 2006 outbursts are similar in terms of brightness and temperature evolution (Orio et al. 2022; Page et al. 2022) suggesting the gross properties of the shock interaction to be similar. The results from VLBI observations also point to the same conclusions. The shock radius at $t \sim 34$ d in the 2021 outburst from VLBI measurements (Munari et al. 2022) is remarkably the same as the shock radius at similar epochs in the 2006 eruption (O’Brien et al. 2006, 2008; Rupen, Mioduszewski & Sokolowski 2008; Sokolowski, Rupen & Mioduszewski 2008). Contrary to a very similar evolution in optical, hard X-ray, and VLBI observations, the soft (0.3–1 keV) X-ray emission during the SSS phase was found to be very different. The SSS emission during the 2021 outburst is 4–5 times fainter than that of the 2006 outburst (Page et al. 2022).

A higher accretion rate can lead to a rapid increase in temperature of the WD surface for a given accreted mass (Prialnik et al. 1982) and result in a weaker nova and SSS emission. However, there are no observational signatures of a difference in accretion rate during

Table 4. Optical depth due to uniform and clumpy circumburst medium during the 2021 and 2006 outbursts.

Time ^a (d)	2021			2006		
	τ_{homo} ($\times 10^{-3}$)	τ_{clumps}	τ_{eff}	τ_{homo}	τ_{clumps}	τ_{eff}
15.0	1.58 ± 0.46	0.38 ± 0.06	0.17 ± 0.03	0.04 ± 0.03	0.30 ± 0.21	0.18 ± 0.10
24.2	0.60 ± 0.19	0.44 ± 0.07	0.20 ± 0.03	0.06 ± 0.05	0.29 ± 0.21	0.20 ± 0.11
33.1	0.59 ± 0.20	0.69 ± 0.11	0.31 ± 0.05	0.11 ± 0.09	0.41 ± 0.33	0.30 ± 0.18
70.4	0.04 ± 0.02	0.52 ± 0.12	0.23 ± 0.05	0.15 ± 0.18	0.21 ± 0.24	0.25 ± 0.22

Notes. ^aThis column indicates the time from the nova outburst, i.e. 2021 Aug 08.5 UT (Munari & Valisa 2021a).

τ_{homo} and τ_{clumps} denote the optical depths due to uniform and clumpy mediums, respectively. τ_{eff} is the effective optical depth (Weiler et al. 2002).

the quiescent intervals prior to 2006 and 2021 outbursts (Orio 1993; Page et al. 2022). The quiescent X-ray luminosities (0.3–10 keV) are $\sim 6 \times 10^{31} \text{ erg s}^{-1}$, orders of magnitude less compared to the expected value of $\sim 10^{36} \text{ erg s}^{-1}$ (Anupama & Mikołajewska 1999; Osborne et al. 2011). A possible explanation for such suppression in quiescent luminosity is the complex (partially covering) absorbing medium in the system. Ness et al. (2023) compared the X-ray grating spectra of 2006 and 2021 outbursts during the SSS phase and concluded that higher absorption in the line of sight is the main reason for the observed lower SSS emission in 2021.

The line-of-sight absorbing material is created due to aspherical mass-loss in the binary system and could have a dependence on the orbital phase (Walder, Folini & Shore 2008; Drake et al. 2009; Orlando, Drake & Laming 2009). The 1985, 2006, and 2021 outbursts occurred at phases 0.32, 0.26, and 0.72, respectively. Simulation results from Booth, Mohamed & Podsiadlowski (2016) showed that a spiral accretion during the quiescent phase builds up material such that there could be more material in the line of sight during the 2021 outburst. The simulation shows a low density at an orbital phase ~ 0.26 , which is during the 2006 outburst. The authors also suggest that the simulated material is clumpy.

We re-visit the differences in the evolution of low-frequency radio light curves in 2006 and 2021 outbursts in light of the results from Ness et al. (2023). The radio emission is the brightest in the 2021 outburst with a peak flux density of $\sim 87 \text{ mJy}$ at 1.4 GHz on $t \sim 15 \text{ d}$ post-outburst (de Ruiter et al. 2023). The 1.4 GHz light curve is sparsely sampled in the 2006 outburst and the peak flux and time from the best-fitting model are $F_p \sim 61 \text{ mJy}$ and $t \sim 15 \text{ d}$, respectively (Kantharia et al. 2007). Assuming similar ejecta and shock properties, these peak flux densities indicate that there are more particles in the synchrotron emitting plasma in 2021 than that of 2006 outburst.

The integrated X-ray count from SSS emission in the 2021 outburst during $t \sim 30\text{--}86 \text{ d}$ is 4–5 times lower than that of 2006 possibly due to higher absorption (Ness et al. 2023). These two observational characteristics point out that the medium in the vicinity of the binary system during the 2021 outburst is relatively denser compared to that of 2006 outburst.

8 SUMMARY

We present low-frequency radio observations of the 2021 outburst of RS Ophiuchi during 23–287 d post-outburst at frequencies 0.15–1.4 GHz. Our main findings are the following:

(i) Radio emission at the observed frequencies are characterized by high brightness temperatures ($10^5\text{--}10^8 \text{ K}$) with an average optically thin spectral index of $\alpha \sim -0.4$, consistent with non-thermal emission process.

(ii) The spectral and temporal evolution of the radio flux measurements are best represented by synchrotron emission that arises due to the interaction of external shock from the nova outburst with the dense wind of the red giant companion. The emission is initially suppressed due to free–free absorption by the uniform and clumpy foreground CBM.

(iii) The mass-loss rate of the red giant has been estimated to be $\dot{M} = 7.5^{+1.5}_{-1.6} \times 10^{-8} M_{\odot} \text{ yr}^{-1}$ for a wind velocity of 20 km s^{-1} , consistent with the mass-loss rates of RGB stars (McDonald & van Loon 2007).

(iv) Comparison of light curves from the 2021 and 2006 outbursts in the 0.15–1.4 GHz radio bands shows that the peak flux densities in the 2021 outburst are 1.5–1.6 times higher than that of the 2006 outburst values. Considering similar shock and ejecta properties of these outbursts as supported by multiwavelength observations (Munari et al. 2022; Orio et al. 2022; Page et al. 2022), we interpret the brighter radio emission in 2021 to be due to a higher particle density in the synchrotron emitting plasma.

Our study suggests that rapid multifrequency radio follow-up observations of recurrent novae are crucial to tie down various absorption processes and infer the properties of shock and CBM.

ACKNOWLEDGEMENTS

We thank the anonymous referee for the comments that helped to improve our manuscript. We thank the staff of the GMRT that made these observations possible. The GMRT is run by the National Centre for Radio Astrophysics of the Tata Institute of Fundamental Research. AJN would like to acknowledge DST-INSPIRE Faculty Fellowship (IFA20-PH-259) for supporting this research. KPS thanks the Indian National Science Academy for support under the INSA Senior Scientist Programme.

DATA AVAILABILITY

The data underlying this article will be shared on reasonable request to the corresponding author.

REFERENCES

- Acciari V. A. et al., 2022, *Nat. Astron.*, 6, 689
 Anupama G. C., Mikołajewska J., 1999, *A&A*, 344, 177
 Bailer-Jones C. A. L., Rybizki J., Fouesneau M., Demleitner M., Andrae R., 2021, *AJ*, 161, 147
 Bode M. F., Harman D. J., O’Brien T. J., Bond H. E., Starrfield S., Darnley M. J., Evans A., Eyres S. P. S., 2007, *ApJ*, 665, L63
 Booth R. A., Mohamed S., Podsiadlowski P., 2016, *MNRAS*, 457, 822
 Cheung C. C. et al., 2022, *ApJ*, 935, 44
 Chevalier R. A., Fransson C., 2006, *ApJ*, 651, 381

- Chomiuk L. et al., 2012, *ApJ*, 761, 173
- Chomiuk L. et al., 2021, *ApJS*, 257, 49
- Chugai N. N., 2010, *Astron. Lett.*, 36, 540
- Das R., Banerjee D. P. K., Ashok N. M., 2006, *ApJ*, 653, L141
- de Ruiter I., Nyamai M. M., Rowlinson A., Wijers R. A. M. J., O'Brien T. J., Williams D. R. A., Woudt P., 2023, *MNRAS*, 523, 132
- De Sarkar A., Nayana A. J., Roy N., Razzaque S., Anupama G. C., 2023, *ApJ*, 951, 62
- Diesing R., Metzger B. D., Aydi E., Chomiuk L., Vurm I., Gupta S., Caprioli D., 2023, *ApJ*, 947, 70
- Drake J. J. et al., 2009, *ApJ*, 691, 418
- Eyres S. P. S. et al., 2009, *MNRAS*, 395, 1533
- Foreman-Mackey D., Hogg D. W., Lang D., Goodman J., 2013, *PASP*, 125, 306
- Greisen E. W., 2003, in Heck A., ed., *Astrophysics and Space Science Library*, Vol. 285, Information Handling in Astronomy – Historical Vistas. Springer-Verlag, Berlin, p. 109
- H. E. S. S. Collaboration, 2022, *Science*, 376, 77
- Hjellming R. M., van Gorkom J. H., Taylor A. R., Sequist E. R., Padin S., Davis R. J., Bode M. F., 1986, *ApJ*, 305, L71
- Kantharia N. G., Anupama G. C., Prabhu T. P., Ramya S., Bode M. F., Eyres S. P. S., O'Brien T. J., 2007, *ApJ*, 667, L171
- Longair M. S., 2011, *High Energy Astrophysics*. Cambridge University Press, UK
- McDonald I., van Loon J. T., 2007, *A&A*, 476, 1261
- Mikolajewska J., Aydi E., Buckley D., Galan C., Orio M., 2021, *Astron. Telegram*, 14852, 1
- Mondal A., Anupama G. C., Kamath U. S., Das R., Selvakumar G., Mondal S., 2018, *MNRAS*, 474, 4211
- Munari U., Valisa P., 2021a, preprint ([arXiv:2109.01101](https://arxiv.org/abs/2109.01101))
- Munari U., Valisa P., 2021b, *Astron. Telegram*, 14840, 1
- Munari U., Valisa P., 2022, preprint ([arXiv:2203.01378](https://arxiv.org/abs/2203.01378))
- Munari U., Giroletti M., Marcote B., O'Brien T. J., Veres P., Yang J., Williams D. R. A., Woudt P., 2022, *A&A*, 666, L6
- Narumi H., Hirose K., Kanai K., Renz W., Pereira A., Nakano S., Nakamura Y., Pojmanski G., 2006, in Green D. W. E., ed., *Proc. IAU Circ.* 8671, RS Ophiuchi. p. 2
- Nayana A. J. et al., 2017, *MNRAS*, 467, 155
- Nayana A. J., Anupama G. C., Banerjee D., Roy N., Singh K. P., Sonith L. S., 2021, *Astron. Telegram*, 14899, 1
- Ness J. U. et al., 2023, *A&A*, 670, A131
- O'Brien T. J. et al., 2006, *Nature*, 442, 279
- O'Brien T. J. et al., 2008, in Evans A., Bode M. F., O'Brien T. J., Darnley M. J., eds, *ASP Conf. Ser. Vol. 401, RS Ophiuchi (2006) and the Recurrent Nova Phenomenon*. Astron. Soc. Pac., San Francisco, p. 239
- Origlia L., Rood R. T., Fabbri S., Ferraro F. R., Fusi Pecci F., Rich R. M., 2007, *ApJ*, 667, L85
- Orio M., 1993, *A&A*, 274, L41
- Orio M. et al., 2022, *ApJ*, 938, 34
- Orlando S., Drake J. J., Laming J. M., 2009, *A&A*, 493, 1049
- Osborne J. P. et al., 2011, *ApJ*, 727, 124
- Page K. L. et al., 2022, *MNRAS*, 514, 1557
- Pandey R., Habtie G. R., Bandyopadhyay R., Das R., Teyssier F., Guarro Fló J., 2022, *MNRAS*, 515, 4655
- Prialnik D., Livio M., Shaviv G., Kovetz A., 1982, *ApJ*, 257, 312
- Rupen M. P., Mioduszewski A. J., Sokoloski J. L., 2008, *ApJ*, 688, 559
- Schaefer B. E., 2010, *ApJS*, 187, 275
- Sokoloski J. L., Rupen M. P., Mioduszewski A. J., 2008, *ApJ*, 685, L137
- Sokolovsky K. et al., 2021, *Astron. Telegram*, 14886, 1
- van Loon J. T., McDonald I., Oliveira J. M., Evans A., Boyer M. L., Gehrz R. D., Polomski E., Woodward C. E., 2006, *A&A*, 450, 339
- Walder R., Folini D., Shore S. N., 2008, *A&A*, 484, L9
- Weiler K. W., Sramek R. A., Panagia N., van der Hulst J. M., Salvati M., 1986, *ApJ*, 301, 790
- Weiler K. W., Panagia N., Montes M. J., Sramek R. A., 2002, *ARA&A*, 40, 387
- Williams D., O'Brien T., Woudt P., Nyamai M., Green D., Titterton D., Fender R., Sivakoff G., 2021, *Astron. Telegram*, 14849, 1
- Zheng J.-H., Huang Y.-Y., Zhang Z.-L., Zhang H.-M., Liu R.-Y., Wang X.-Y., 2022, *Phys. Rev. D*, 106, 103011

This paper has been typeset from a $\text{\TeX}/\text{\LaTeX}$ file prepared by the author.